Chemistry & Biology
Article

Electron Hole Flow Patterns through the RNA-Cleaving 8-17 Deoxyribozyme Yield Unusual Information about Its Structure and Folding

Edward K.Y. Leung[1] and Dipankar Sen[1,*]
[1] Department of Molecular Biology & Biochemistry, Simon Fraser University, Burnaby, British Columbia, V5A 1S6, Canada
*Correspondence: sen@sfu.ca
DOI 10.1016/j.chembiol.2006.11.006

SUMMARY

DNA double helices have been shown to conduct electron holes over significant distances. Here, we report on the hole flow patterns within a more intricately folded DNA complex, the 8-17 deoxyribozyme bound to a DNA pseudosubstrate, incorporating three helical elements and two catalytically relevant loops. The observed hole flow patterns within the complex permitted a quantitative assessment of the stacking preferences of the three constituent helices and provided evidence for significant transitions within the complex's global geometry. The patterns further suggested varying levels of solvent exposure of the complex's constituent parts, and revealed that a catalytically relevant cytosine within the folded complex exists in an unusual structural/electronic environment. Our data suggest that the study of charge flow may provide novel perspectives on the structure and folding of intricately folded DNAs and RNAs.

INTRODUCTION

Over the past two decades, intensive research has shown that DNA double helices, in aqueous solution, are able to conduct electrical charge, albeit modestly (reviewed in [1, 2]). Two classes of charge conduction have been studied: (1) classes in which the carrier of charge is a nucleobase radical cation (an "electron hole"); and (2) classes in which it is a radical anion (an "excess electron"). Of the two, hole transfer has been studied in greater depth; in this paper, we use the term "charge transfer" to refer exclusively to hole transfer. Charge flow via hole transfer in DNA can conveniently be initiated by photoexcitation of a sensitizer moiety, such as anthraquinone (AQ), covalently linked and pi stacked upon the end of a double helix. An initial nucleobase radical cation generated within the helix can propagate along the helix over relatively long distances (~200 Å) [3–5]. Of the four DNA bases, guanine (G) is the most easily oxidized. (The guanine radical cation, $G^{\bullet+}$, is the most stable of the four possible radical cations.) Both hopping and superexchange mechanisms have been invoked to account for the observed charge transfer (and, indeed, both appear to be relevant, at different distance scales [6–8]); a recent refinement of the hopping model, the "phonon-assisted polaron-like hopping" model, most successfully accounts for the hole conduction [4, 5]. Any guanine base that transiently hosts the mobile radical cation is susceptible to a side reaction with water (or, in some instances, dissolved oxygen), leading to the formation of modest levels of guanine oxidation products such as 8-oxoguanine or diaminooxazalone (reviewed in [9]). The formation of these products provides a convenient biochemical handle for tracing the charge flow path though DNA, since treatment with hot piperidine breaks the DNA strand at such sites.

The susceptibility of any specific guanine within a double helix to charge flow-related oxidation depends somewhat on the sequence context of the guanine [1–3]; stretches of adjacent guanines, such as GG or GGG, are particularly susceptible to oxidation, with the 5′-most guanine of the stretch the most oxidizable [1–3, 9]. Densitometry trace of charge flow-dependent DNA cleavage ("CFDC") provides a convenient and quantitative means for mapping charge flow through double helices as well as simple assemblages of helices, such as DNA three-way and four-way helical junctions [10–13]. Not surprisingly, the integrity of pi stacking between adjacent bases or base pairs strongly influences the efficiency of hole conduction; where a pi stack is perturbed (such as with mismatches or bulges), hole migration efficiency diminishes notably [14, 15].

Recently, we have reported the construction and charge conduction properties of "deoxyribosensors," structural variants of classic three-way junctions, which change conformation upon binding specified "analytes"or "ligands," such as adenosine or argininamide [10, 16]. Figure 1A shows the secondary structure of a typical deoxyribosensor construct ("ArgA1.3") originally designed to sense argininamide binding [16]. Charge flow was initiated by photoexcitation of an AQ tethered to the end of the "AQ stem," and charge flow into the "signal stem" could then be monitored by measurement of oxidative damage, leading to DNA cleavage at a GGG motif located within that arm. In testing different deoxyribosensor constructs (which varied only in the sequences immediately bordering the junction itself), it was found that in some constructs

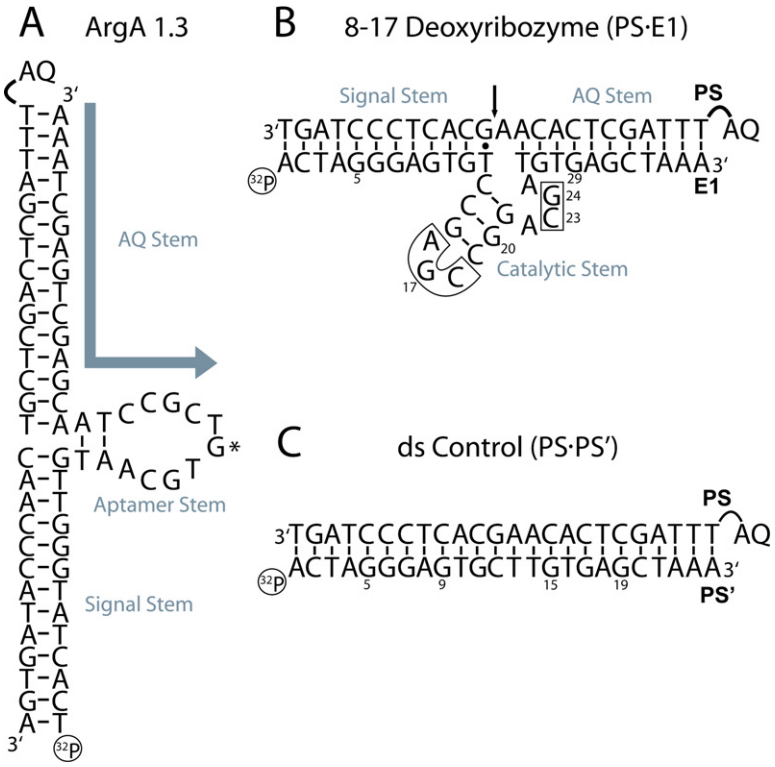

Figure 1. DNA Complexes Studied Using Charge Transfer

(A) An argininamide biosensor (ArgA 1.3) studied by Sankar and Sen [16]. The gray arrow indicates the preferred path of charge flow, from the AQ stem to the aptamer stem. The guanine labeled by an asterisk (*) in the aptamer stem was particularly prone to charge flow-dependent oxidative damage.

(B) E1, the 8-17 DNAzyme construct used in this paper, shown bound to its all-DNA pseudosubstrate (PS). The PS strand has anthraquinone (AQ) covalently linked to its 5′ end. The arrow indicates the site of cleavage if a true substrate were bound to the DNAzyme. The boxed nucleotides in E1 have been reported to be important for the catalysis by E1.

(C) A double-stranded positive control of PS bound to its exact Watson-Crick complement, PS′.

charge flowed from the AQ arm mainly or exclusively to the signal arm, while in other constructs it flowed to the aptamer arm. Charge flow patterns could therefore, in principle, be used to monitor helix-stacking preferences in the different deoxyribosensor constructs [16]. In the ArgA1.3 construct, CFDC appeared to localize mainly in the aptamer arm rather than the signal stem [16]. A notable finding was that a guanine located at the apex of the aptamer loop (shown with an asterisk in Figure 1A) showed strong oxidative damage at all argininamide concentrations tested. A high-resolution NMR structure of the argininamide aptamer bound to its ligand, however, has shown this apical guanine to be both unstacked and jutting out into the solvent [17].

It is possible to interpret the level of CFDC at any DNA site as the product of two distinct processes: (1) the efficiency of charge transfer to and from the guanine at that site versus (2) the efficiency of the water reaction with the $G^{\bullet+}$ species generated at that site. In the case of the high level of CFDC seen at the apical guanine of Arg1A.3, we postulate that the lack of this guanine's pi stacking upon its neighboring bases should imply a poor step (1), i.e., the rate of formation of its radical cation; nevetheless, step (2) should be relatively fast, i.e., once formed, this solvent-exposed $G^{\bullet+}$ should react efficiently with water.

The above-described studies with deoxyribosensors raised the following interesting points: (1) charge flow patterns from a fixed charge source (the AQ stem) to competing recipient helices appeared to provide a "stacking partner index" for the different helix pairs; and (2) high CFDC levels could be observed both in guanines that were known to be intrahelical (for instance, the 5′-most G of a GGG sequence) and, at least in one instance, to a guanine that was unstacked yet exposed to the solvent. These findings suggest that a global study of charge flow patterns through complexly folded DNAs might provide interesting kinds of structural information, including helix-stacking preferences and, potentially, the folding patterns of segments or domains within the folded DNA.

Ribozymes and deoxyribozymes (DNAzymes) are nucleic acid molecules capable of catalyzing a wide variety of different chemical reactions, including RNA cleavage. At least five small, RNA-cleaving ribozyme motifs—the Hammerhead, Hairpin, Hepatitis Delta Virus (HDV), Varkud Satellite (VS), and the GlmS—are known to exist in nature [18, 19]. In addition, a number of small, RNA-cleaving deoxyribozymes (DNAzymes) have been isolated by using in vitro selection from random-sequence DNA pools; these include the 8-17 and 10-23 DNAzymes [20, 21], the bipartite DNAzyme [22], and a number of others (reviewed in [23, 24]), all of which are roughly comparable in size and catalytic activity to the naturally occurring small ribozymes. Crystal structures for a number of the small ribozymes have been reported recently (reviewed in [25]); however, no such high-resolution structural information exists on the small deoxyribozymes. Nevertheless, the structure and folding of a number of these DNAzymes, notably the 8-17, have been studied intensively, by using a variety of chemical and biochemical probes, fluorescence resonance energy transfer, model building, and saturation mutagenesis [26–29]. The 8-17, the smallest of the RNA-cleaving DNAzymes, was reported, on the basis of

sequence diversity observed between different selected clones, to have a catalytic core (shown in Figure 1B) composed of a short (3 bp), double-stranded stem terminating in an invariant AGC terminal loop and a key unpaired region (4–5 nt) whose sequence conformed to the sequence consensus WCGR (where W = A or T and R = G or A) or to WCGAA [21]. The original ACGA-looped 8-17 characterized by Santoro and Joyce [21] required magnesium ions for its catalytic activity. More recent studies on 8-17 sequence variants have found that some work optimally in calcium, manganese, lead, or zinc [27, 30–32]. Figure 1B illustrates a typical 8-17 construct, "E1" (with an ACGA internal loop, of the WCGR type), bound to a DNA pseudosubstrate, "PS." (The 8-17 DNAzyme cleaves all-RNA substrates, as well as DNA substrates with a single ribonucleotide embedded at the cleavage site; the PS pseudosubstrate lacks that ribonucleotide.) Systematic mutagenesis of the 8-17 catalytic core, by using natural as well as non-natural base analogs, has provided a detailed picture of the involvement of individual residues and functional groups within the 8-17 catalytic core in hydrogen bonding and catalysis [29]. At the same time, fresh in vitro selection experiments from random DNA sequences have yielded, repeatedly, DNAzymes that belong to the 8-17 family [27]. This latter observation has permitted the identification of certain nucleotides in the catalytic core (shown as boxed within Figure 1B) as being indispensable for catalysis.

In examining the secondary structure of E1-PS (Figure 1B), we were struck by the resemblance of its secondary structure to that of the ArgA1.3 deoxyribosensor (Figure 1A). Both are variants of standard DNA three-way junctions. (ArgA1.3 did not include a 2–3 nt bulge at the junction; however, a number of related sensors examined by Sankar and Sen [16] did.) We therefore hypothesized that a study of charge transfer through the E1-PS complex, starting from a fixed point in its structure (the covalently linked AQ moiety stacked upon the end of the AQ stem; Figure 1B), might supply interesting new information about the structure and the folding properties of the 8-17 DNAzyme.

RESULTS AND DISCUSSION

Helical Stacking Relationships

To study charge transfer patterns through the E1-PS complex, we selected a pseudosubstrate sequence (and, correspondingly, the sequences of the two substrate-binding arms of E1) that incorporated at least 1 GC bp per every 2–4 bp to facilitate hole transfer within the AQ and signal stems (Figure 1B). A GGG hole trap was specifically placed in the signal stem of the complex; a GG trap was also naturally present in the 3 bp stem in the catalytic core (catalytic stem).

The first question we asked was whether charge from the AQ stem flowed preferentially to the signal stem or into the catalytic core of the E1-PS complex. For comparison, we also studied charge transfer through a double-helical control, PS-PS′ (Figure 1C), which consisted of the PS oligonucleotide fully Watson-Crick base paired to a complementary oligonucleotide, PS′. Figure 2A shows denaturing gels highlighting the CFDC data obtained. Lanes 1–4 show a number of control experiments on the E1-PS complex: lane 1 shows the results of piperidine treatment of 5′-^{32}P end labeled but unirradiated single-stranded E1; lane 2 shows the E1-PS complex with appended AQ, irradiated with light, but not treated with piperidine; lane 3 shows the AQ-derivatized E1-PQ complex, treated with piperidine without having been irradiated first; and lane 4 shows the E1-PS complex lacking an appended AQ, irradiated and then treated with piperidine. In all of the above, it is the E1 strand that is 5′-^{32}P labeled. The absence of DNA cleavage bands in all four controls confirms that CFDC requires DNA constructs that are (1) derivatized with AQ, (2) have been irradiated with 335 nm light, and (3) have been treated with hot piperidine. Lanes 8–10 show CFDC of the E1-PS complex (with the E1 strand 5′-^{32}P labeled) dissolved in, respectively, 10 mM Tris (pH 7.4), 0.1 mM EDTA (TE buffer), TE plus 50 mM NaCl, and TE, 50 mM NaCl, plus 1 mM $MgCl_2$. Under the last of these conditions, E1 is, of course, catalytically active with a cleavable substrate [33]. Under all three conditions, significant CFDC can be seen both in the signal stem (G5–T12) and in the catalytic core (C13–A25). If we make the assumption that the efficiency of stacking between a given pair of helices, X and Y, relative to pair X and Z, is reflected in the relative efficiencies of charge transfer X → Y and X → Z, then the CFDC data suggest that, in the E1-PS complex, over the experimental timescale, the AQ stem experiences stacking with both the signal stem and the catalytic core (suggesting a relative dynamic, or floppy, arrangement of the helices). Since the sequences of these two "charge-accepting" elements are not the same, to obtain a quantitative sense of the effectiveness of signal stem-AQ stem stacking in E1-PS, we compared it with the stacking of the same helix pair within the duplex control, PS-PS′, under identical solution conditions (Figure 1C). Densitometry of the signal at G5 (as a percentage of the total counts in lane 5, Figure 2A) of PS-PS′ was measured to be ~7% of the total in that lane, whereas the counts at G5 of E1-PS (lane 10, Figure 2A) were ~2% of the total in that lane. (By contrast, the analogous AQ stem guanines, G19 in PS-PS′ and G31 in E1-PS, had comparable levels of damage.) Charge transfer (and stacking) between the AQ and signal stems therefore appears to be 3- to 4-fold less efficient in E1-PS than in a continuous double helix of the same sequence. A more detailed analysis of the global structural changes suggested by these data is given below.

A most unexpected result, however, was the high level of CFDC at a cytosine, C23 (lanes 9 and 10, Figure 2A). C23 has been reported in a number of studies to be a key residue for 8-17 catalysis [21, 27–33]. This gel band was especially prominent in lane 10, where E1-PS was folded in the presence of magnesium under conditions that support catalysis. Cytosine is significantly harder to oxidize than guanine or adenine (E° = 1.29 V versus NHE for the free ribonucleotide rG, but 1.6 V for rC [9]); nevertheless, all four DNA bases, including cytosine and thymine, remain

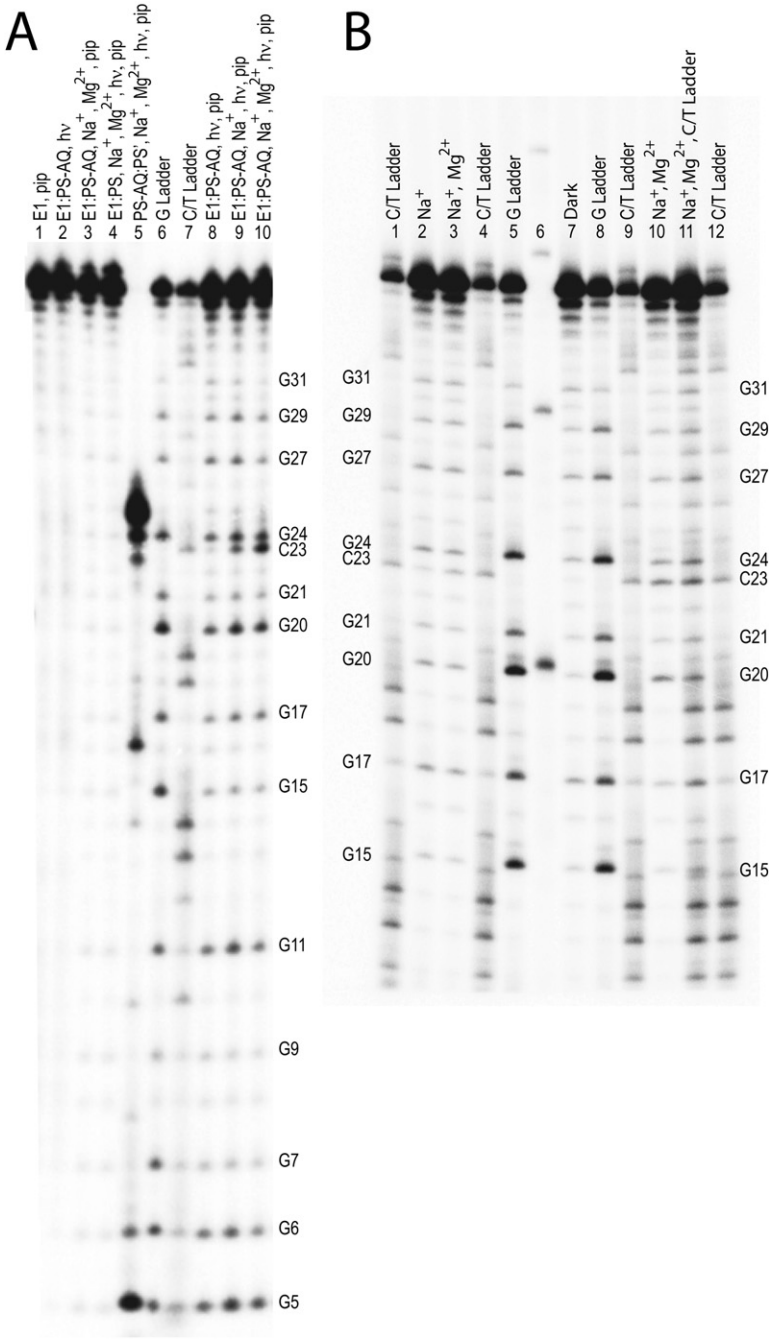

Figure 2. Denaturing Gels Showing Patterns of Charge Flow-Dependent DNA Strand Cleavage

(A) Charge flow patterns of the E1-PS and the PS-PS′ complexes, alongside controls. Lane 1: E1 alone, treated with piperidine; lane 2: AQ-derivatized E1-PS, irradiated but not treated with piperidine; lane 3: AQ-derivatized E1-PS, folded in the presence of sodium and magnesium salts, unirradiated, but treated with piperidine (the "Dark" control for E1-PS); lane 4: E1-PS, not derivatized with AQ, folded in the presence of sodium and magnesium salts, irradiated, and treated with piperidine; lane 5: PS′-PS, derivatized with AQ, folded in the presence of sodium and magnesium salts, irradiated, and treated with piperidine; lane 6: a Maxam-Gilbert G ladder; lane 7: a Maxam-Gilbert C/T Ladder; lane 8: E1-PS-AQ, derivatized with AQ, irradiated in a low-salt buffer, and treated with piperidine; lane 9: E1-PS-AQ, folded in the presence of only sodium salts, irradiated, and treated with piperidine; lane 10: E1-PS-AQ, folded in the presence of sodium and magnesium salts, irradiated, and treated with piperidine.

(B) CFDC patterns of E1-PS (derivatized with AQ), folded under different conditions, irradiated, and treated with piperidine, compared with Maxam-Gilbert C/T ladders. Lanes 1, 4, 9, and 12: the C/T ladder; lane 2: E1-PS-AQ, folded in the presence of sodium salts only, irradiated, and treated with piperidine; lanes 3 and 10: E1-PS-AQ, folded in the presence of sodium and magnesium salts, irradiated, and treated with piperidine; lanes 5 and 8: a Maxam-Gilbert G ladder; lane 6: a 10 nt ladder; lane 7: "Dark" (unirradiated) E1-PS-AQ, folded in the presence of sodium and magnesium salts, and treated with piperidine; lane 11: E1-PS-AQ, folded in the presence of sodium and magnesium salts, irradiated, and treated with piperidine, mixed with C/T ladder.

oxidizable by photoexcited AQ, whose reduction potential is 2.0 V versus NHE [34]. Moreover, it has been demonstrated experimentally [35, 36] that in the process of hopping between guanines within DNA double helices, the electron hole does physically localize on adenine and cytosine bases in the form of the radical cations $A^{\bullet+}$ and $C^{\bullet+}$, with concomitant oxidative transformation of those bases (demonstrated, in these reports, by monitoring a fast ring opening of cyclopropyl groups covalently appended to the C and A bases) [35, 36]. By contrast, CFDC at cytosines has not been reported from charge conduction studies on double-helical DNA, owing, presumably, to the relatively slow kinetics of the water reaction of intrahelical $C^{\bullet+}$ species [34–36]. However, it is not at all inconceivable that $C^{\bullet+}$ species at relatively unstacked and solvent-exposed locations should not undergo oxidative damage via the water reaction. A candidate oxidization product of cytosine, 5-hydroxycytosine, is known to be labile upon treatment with hot piperidine [9].

We investigated whether the C23 CFDC gel band genuinely arose from C23, rather than being a satellite band from aberrant cleavage at the neighboring A22. (Based on examination of the details of Maxam-Gilbert DNA cleavage chemistry, this band could not be an aberrant cleavage

product of G24.) We used long denaturing gels to compare the gel mobility of the C23 CFDC band with that of a C23 band in a Maxam-Gilbert cytosine reaction ladder. (Both CFDC and the Maxam-Gilbert sequencing methodology utilize hot piperidine workup to effect cleavage of the base-sugar glycosidic bond and the subsequent β elimination.) The band mobilities were compared by (1) running them in adjacent lanes (lanes 2 and 3 versus lanes 1 and 4, Figure 2B), as well as (2) mixing the CFDC and Maxam-Gilbert ladders together and running the mixture in a composite lane (lane 11, Figure 2B). In both instances, the mobility of the C23 CFDC band and that of C23 in the sequencing ladder were indistinguishable from one another, indicating that the C23 CFDC band genuinely arose from the standard piperidine-catalyzed chemistry at the modified (oxidized) C23 site in the E1 DNA.

It is known that photoexcitation of AQs in aqueous solution generates low concentrations of singlet oxygen [4]. Could the CFDC at C23 have arisen from the direct reaction of that cytosine with diffusible singlet oxygen? We have found no precedent in the literature, including in a paper published this year, for reactivity of singlet oxygen with cytosine within DNA [37–40]. A recent review has stated explicitly that "$^1O_2$ oxidizes the guanine base of DNA exclusively" [39]. Moreover, Henderson et al. [4] have studied and ruled out any role of diffused singlet oxygen even in guanine damage within an AQ-initiated DNA charge transfer system like ours (using experimental conditions very similar to ours). A singlet oxygen origin of the C23 cleavage band is, in our perception, rendered even more unlikely given that singlet oxygen, generated 10 bp or more away from C23, at the AQ moiety, would react with such exquisite specificity with C23 but with no other cytosine within the E1 strand. (Even C32, located 4 bp away from the AQ, doesn't show even a trace of cleavage [Figure 3].)

As discussed above, the unusual CFDC at C23 suggests, at minimum, that this cytosine is located in an unusual local environment within the folded E1-PS complex. What kind of environment might that be? One possibility is that the oxidation potential for this cytosine might be lower than the usual; or, it may enjoy an unusual exposure to and reactivity with the solvent. The oxidation potential might be modulated in a number of different ways: for instance, if C23 participated in net hydrogen bond donation (electron density acceptance), or if it existed substantially in a deprotonated state. The latter scenario, if true, might underlie this cytosine's catalytic importance, in analogy with ribozymes such as HDV, in which cytosine residues have been shown to participate in acid-base catalysis [41, 42].

To test some of these possibilities, we constructed a C23T point mutant of E1. The mutant DNAzyme, E1(T), was found to be catalytically inactive, in agreement with prior biochemical data [29]. Nevertheless, charge transfer experiments on the E1(T)-PS complex gave a strikingly similar CFDC pattern to that of the original E1-PS complex, including a notable CFDC at the mutated T23 residue (data not shown). Thymine is even more resistant to oxidation than is cytosine (1.7 eV relative to 1.6 eV; [9]), and the two nucleobases have significantly different hydrogen

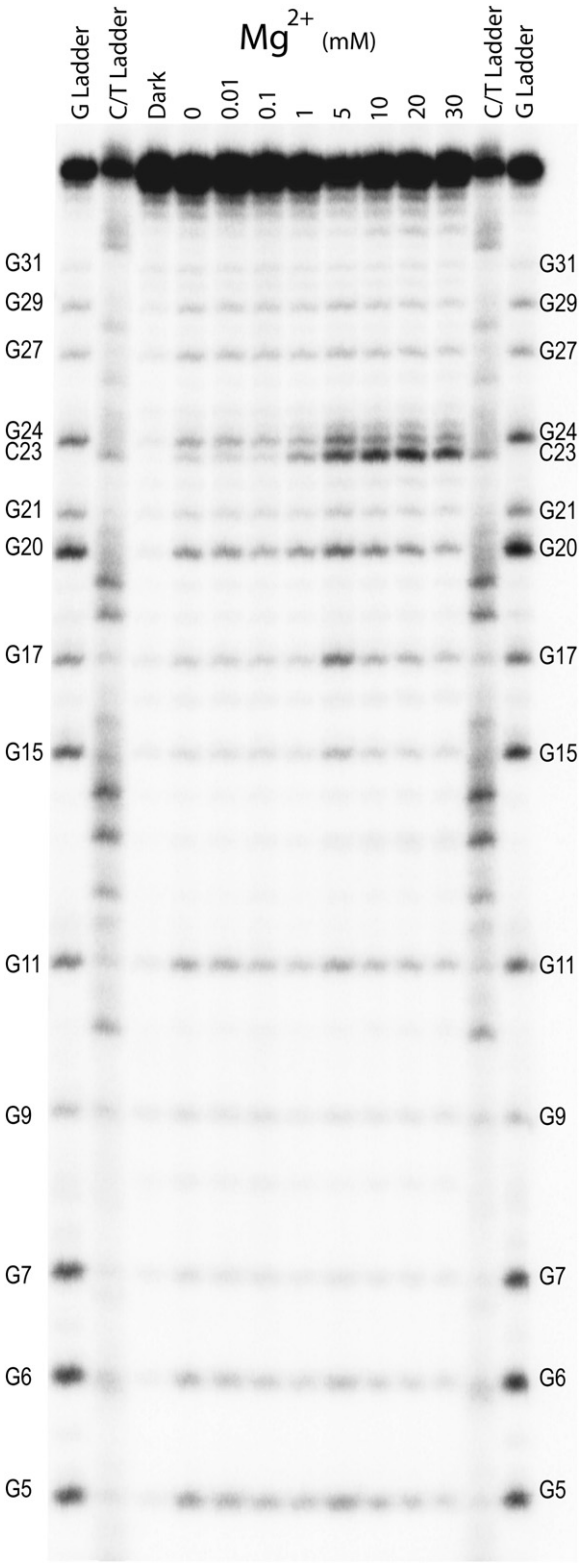

Figure 3. Magnesium Titrations of E1-PS
CFDC patterns of E1-PS-AQ, folded in the presence of sodium and increasing concentrations of magnesium.

bonding, metal binding, and acid-base properties. Nevertheless, the similarity in the CFDC patterns of the E1-PS and E1(T)-PS complexes suggests that the CFDC seen at C23 (and T23) is unlikely to be attributable to unusual hydrogen-bound or metal-bound states or, indeed, acid-base properties of C23. (The C23T mutation should strongly perturb or ablate all of these properties, with the possible exception of metal coordination by the 2-keto oxygen shared by C and T.) Indeed, on the basis of their extensive mutagenesis study, Peracchi and colleagues have proposed that the catalytically important C23 does not participate as an acid-base catalyst [29]. The most parsimonious explanation for the high level of CFDC at C23 (or T23) is therefore the high solvent accessibility of the nucleobase. Below, we describe additional experiments to test that hypothesis.

Charge Flow Patterns as a Function of Magnesium Concentration

The above-described experiments, shown in Figures 2A and 2B, had been carried out in buffers that either lacked divalent cations (i.e., conditions in which the DNAzyme would be catalytically inactive) or contained 1 mM Mg^{2+} (in which it would be active). We now studied the charge flow patterns through E1-PS as a function of magnesium concentration (0–30 mM). Figure 3 shows a gel of these experiments; it can be seen that at certain bases (such as at G27 and G29, both in the AQ stem), CFDC levels remain more or less constant across the magnesium range, whereas significant changes occur in others (mostly notably in C23 and G24). To obtain a more quantitative understanding of the changes in CFDC patterns, each gel band was quantitated, and a "damage ratio" was calculated for it. This was defined as the CFDC intensity at a nucleobase, "N," in a given lane, divided by the intensity of G29 in the same lane (after correction for background, "dark" intensities, obtained from the "dark" lane, Figure 3). G29, located close to the activating AQ in the AQ stem, was chosen as the reference base because its CFDC values (0.57% ± 0.17% of the total intensity in a given lane) were relatively insensitive to the range of Mg^{2+} concentrations.

Figure 4A highlights specific guanines within the catalytic core and in the signal stem of E1-PS whose CFDC profiles provided interesting glimpses into the folded structure and structural transitions of the DNAzyme-substrate complex. We first compared G20, 5′-most of a GG sink in the 3 bp stem in the catalytic stem, and G5, 5′-most of the GGG sink located in the signal stem. Figure 4B plots the damage ratios of G5 and G20 as functions of magnesium concentration (the plotted data represent the average of six independent sets of measurements). Both G5 and G20 showed moderately high damage ratios (>2) across the magnesium concentration range examined. The G20 damage ratio increased notably with increasing magnesium and reached a maximum at ~4 mM Mg^{2+}, before dropping at higher magnesium concentrations. By contrast, G5 showed a very modest variation across the magnesium range. Broadly, the data shown in Figure 3 and plotted in Figures 4B and 4C reinforced our earlier conclusion about the absence of a preferred stacking partner for the AQ stem, and this appeared to hold across the magnesium concentration range examined. However, the striking modulations in the Mg^{2+}-dependent damage ratios of G20 suggested significantly different tertiary structures of the E1-PS complex in the different magnesium regimes. The relative constancy of the damage ratios of the AQ stem guanines, G27 and G29, indicates that magnesium itself does not promote CFDC; therefore, the G20 damage ratio increases in the 100 μM–5 mM Mg^{2+} range as well as the subsequent drop at >5 mM Mg^{2+} almost certainly reflect changing degrees of stacking between the catalytic stem and the AQ stem.

Interestingly, Liu and Lu [26] have recently used three-way fluorescence resonance energy transfer (FRET) experiments to propose a two-step change in the tertiary structure of a zinc-responsive ("17E") variant of the 8-17 DNAzyme upon titration with zinc. Although the differences in the E1 and 17E DNAzyme variants, and also in the divalent cation used, prevent a one-on-one comparison of the implications of our CFDC data with their FRET results, some striking points of correspondence can nevertheless be found. According to Liu and Lu, the 17E DNAzyme-substrate complex has three distinct tertiary structure regimes: at <19 μM zinc, in the 19–260 μM zinc range, and at >260 μM zinc. Only in the 19–260 μM zinc range do the AQ equivalent and the catalytic stems of the 17E complex enjoy a degree of coaxiality. In other words, the two stems are poorly coaxial at low zinc concentrations, evolve to greater coaxiality, and are poorly coaxial again at high zinc concentrations. Our data for the G20/G29 damage ratios, plotted in Figure 4B, indicate, qualitatively, a similar pattern of tertiary structure transitions, with low damage ratios (and coaxial stacking) at <100 μM magnesium, relatively high damage ratios (and stacking) in the 100 μM–5 mM range, then poor stacking at >5 mM magnesium. Intrinsic differences in DNA-binding affinities between zinc and magnesium cations may account for the differences in the two cation concentrations required to effect the structural transitions.

Whereas comparison of damage ratios of the intrahelical guanines (G5 and G20, above) provided insights into changes of helical stacking and of the tertiary structure of the E1-PS complex, the catalytically implicated "loop" residues C23 and G24 as well as the "apical" G17 showed different damage ratio trends from each other. Figure 4C shows that G17 had a low damage ratio (1–2) across the magnesium concentration range tested. This pattern is rather different from that of the heavily damaged apical guanine of the deoxyribosensor ArgA 1.3 (Figure 1A; [16]), suggesting that unlike the latter, G17 is not extruded out into the solvent. Indeed, on the basis of extensive mutagenesis experiments, Peracchi and colleagues have proposed that both A16 and G17 participate in an extensive network of hydrogen bonding with yet undefined partners within E1-PS [29]. Li and colleagues have even proposed that these two purines may be involved in stacking interactions with nucleotides at the cleavage site of the substrate [27].

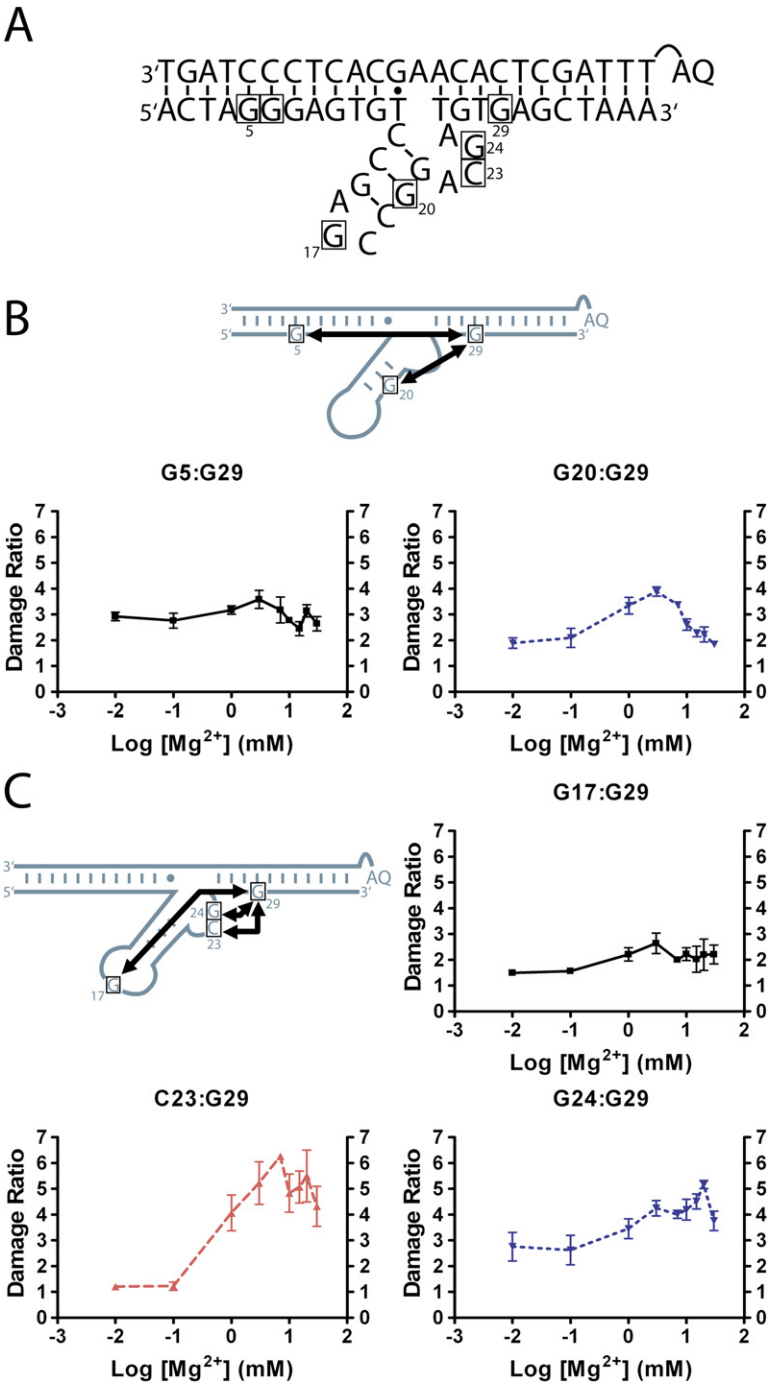

Figure 4. Damage Ratio Analyses at Selected Nucleotides

(A) Damage ratio analyses of key stem and loop nucleotides (shown in boxes) of E1-PS.

(B) Charge flow between intrahelical guanines. The normalized percent damaged of each nucleotide was divided by the percent damage to the reference nucleotide (G29). Error bars shown represent one standard deviation.

(C) Damage ratio analysis for loop bases. Error bars shown represent one standard deviation.

The damage ratios of C23 and G24, however, were very different from those of G17 (Figure 4C). G24 maintains a relatively high damage ratio (~3) even at low (10 μM) magnesium, while at 10 mM magnesium, the damage ratio rises to ~5. The behavior of C23 is particularly striking: from a low damage ratio of ~1 (albeit higher than that of any other cytosine in the E1-PS complex; Figure 3) it rises significantly (with half-maximal height reached at ~1 mM magnesium) to a very high damage ratio of 5–6 at ~10 mM Mg^{2+}. Such a two-state behavior of the C23 damage ratio likely indicates a local folding/structural transition of the ACGA bulge loop at ~1 mM Mg^{2+}.

Ascorbate-Mediated Quenching of Solvent-Exposed Guanine Radical Cations

As discussed in the Introduction, the level of observed damage at a particular nucleobase within a complexly folded nucleic acid reflects a balance between the rate of charge flow into, and out of, that base relative to the rate of water reaction of the resulting radical cation. Given

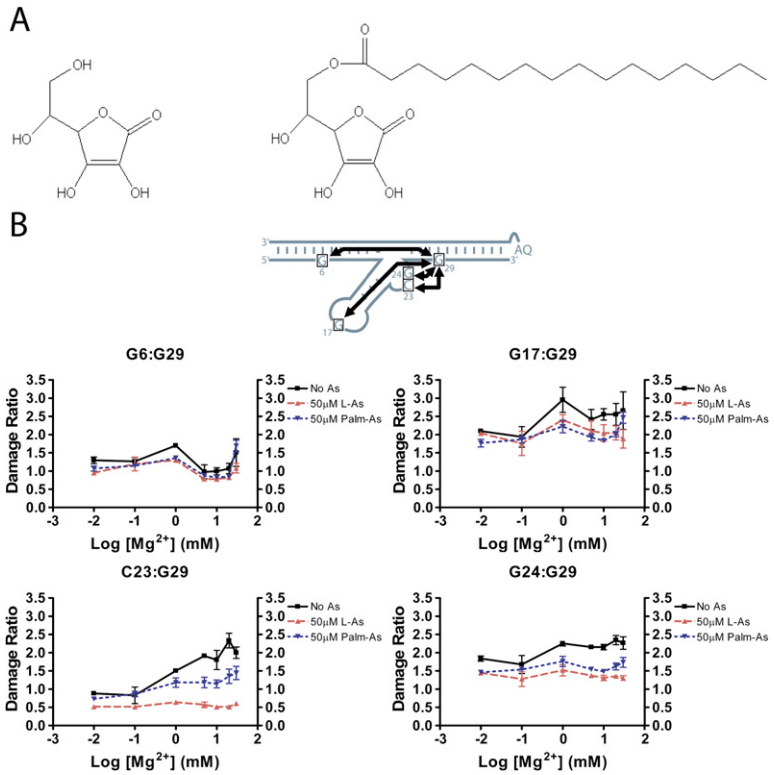

Figure 5. Charge Flow Quenching in the Presence of L-Ascorbic Acid and L-Ascorbic Acid-6-Palmitate

(A) The chemical structures of L-ascorbic and L-ascorbic acid-6-palmitate.

(B) Damage ratio analyses were done on reactions containing no ascorbic acid (solid lines); 50 μM L-ascorbic acid (long, dashed lines); and 50 μM L-ascorbic acid-6-palmitate (short, dashed lines). The above-described data were all obtained from experiments carried out in the presence of 0.185% DMSO; hence, the absolute magnitudes of these damage ratios are lower than those shown in Figures 4B and 4C, which report data measured in the absence of DMSO. Error bars shown represent one standard deviation.

that, it should be possible to distinguish between highly oxidized guanines that are located within helices from those that are extrahelical and more significantly exposed to the solvent. We speculated that enriching the solvent with reducing agents might help to quench the $G^{\bullet+}$ species and, in turn, prevent the water reaction and oxidative damage; one might expect such reductive quenching to be more efficient at solvent-exposed guanines than at intrahelical guanines. To test whether this was a practical strategy, we examined a number of reducing agents, including β-mercaptoethanol, dithiothreitol, reduced glutathione, and ascorbic acid, on a test DNA substrate (a short double helix, terminating in a GGA triloop). We found that ascorbic acid, at concentrations of 50–100 μM, reduced guanine damage preferentially at the apical rather than intrahelical guanines (unpublished data).

For the purpose of probing the E1-PS complex, we speculated that ascorbate itself (Figure 5A, left) might be a small enough molecule to reach and quench even intrahelical $G^{\bullet+}$ species, at certain locations, to a relatively high degree; for that reason, we also explored the effect of a more hindered derivative of ascorbic acid, ascorbic acid-6-palmitate (Figure 5A, right). Figure 5B shows magnesium dependence plots for the damage ratios (averaged over four independent experiments) at the helical G6, at the "apical" G17, as well as for C23 and G24.

The first interesting observation from these dependences was in the positive controls (magnesium dependences measured in the absence of either ascorbate compound, shown as "no ascorbate" in Figure 5B). Owing to the necessity of preparing ascorbic acid-6-palmitate stock solutions in DMSO, the irradiation buffers used for all of the data reported in Figure 5B included 0.185% (v/v) DMSO. While the "no ascorbate" damage ratios for G6 and G17 were comparable in the absence and presence of DMSO (Figures 4B and 4C; the G17 data from Figures 4C and 5B may be compared), those for C23 and G24 decreased notably in the presence of DMSO (Figure 5B) relative to the absence of DMSO (Figure 4C). DMSO is a noted radical scavenger [43, 44] and, at low concentrations, it appears to impact the CFDC at C23 and G24, but not at the intrahelical G6, nor at the extensively hydrogen-bonded G17 [29]. The additional presence of 50 μM ascorbate, or ascorbic acid-6-palmitate, carried these same trends even further (Figure 5B). Damage ratios at G6 remained relatively insensitive to the presence of either ascorbate compound, while the tertiary structure-implicated G17 showed modest decreases. G24 and C23, however, showed dramatic lowering of their damage ratios (with damage at C23 reduced almost to background levels in the presence of 50 μM ascorbate). For both C23 and G24, ascorbate was more effective at $G^{\bullet+}$ quenching than the bulkier ascorbic acid-6-palmitate, and this may reflect our original presumption that the bulkier compound may access only those nucleobases highly exposed to the solvent. Based on its efficiency of quenching, one may postulate that the degree of solvent exposure of C23 is, if anything, greater than that of G24.

These DMSO- and ascorbate-quenching data are, once again, fully consistent with the mutagenesis data of Peracchi et al. [29], who had reported G17 to be involved in "a network of functionally important hydrogen bonds." Our

data indicate that G17 appears to be no more "solvent exposed" than a typical intrahelical guanine. By contrast, C23 and G24 do appear to be significantly solvent exposed, in agreement with prior mutagenesis and biochemical data [29].

Conclusions

The experiments reported here support the idea that the study of charge flow patterns (and the patterns of solvent-based quenching of such charge flow) through a folded nucleic acid complex provides an interesting new, to our knowledge, approach for obtaining valuable structural and electronic information about the complex. Our exploration of the small 8-17 DNAzyme, bound to its substrate, has shown that this simple, gel-based method supplies information not easily obtained by more established methods such as chemical and enzymatic probing, mutagenesis, phylogenetic mapping, as well as flouresscence and other spectroscopic methods. We have shown here that charge flow patterns are able to provide, at minimum, the following types of information about the 8-17 DNAzyme (and, by extension, other folded DNAs): (1) insights into the coaxial stacking preferences of three double-helical elements, information that, in turn, can be used to model the global structure of the folded enzyme-substrate complex; (2) the unusual charge flow-dependent reactivity of certain non-guanine bases, such as the catalytically relevant C23 residue of the 8-17 DNAzyme; (3) the sensitive monitoring of structural transitions of different segments or domains of the folded DNA in response to changing solution conditions, such as magnesium concentration; and (4) insight, based on the quenching patterns of charge flow-generated radical cations, into the extent of solvent exposure of different residues within the folded complex. Further studies, including those to be carried out on RNA (RNA-DNA heteroduplexes and chimeras have been shown to conduct charge [45, 46]; our own unpublished work has shown the same to be true for double-stranded RNAs), will permit us to develop deeper insights into the specific implications of charge flow-related reactivities of individual bases, and such studies should ultimately reinforce a versatile new, to our knowledge, approach for studying DNA and RNA structure and folding.

SIGNIFICANCE

The conduction of electron holes by double-helical DNA is a well-established field. Here, we have studied the hole conduction properties of a complexly folded DNA, the 8-17 deoxyribozyme bound to a pseudo-substrate, which incorporates a number of helices, junctions, and loops. We find that this intricately folded deoxyribozyme-substrate complex shows a number of remarkable conduction features, including the high conduction-related oxidative damage of certain key nucleobases known to be important for 8-17 catalysis. Quantitative assessments of hole transfer efficiencies through the three constituent helices give measures of their stacking propensities, and hole quenching experiments that we carried out with dissolved ascorbate reveal the degrees of solvent exposure of key nucleobases. Our data suggest that the study of charge flow, as a general method, may provide novel perspectives on the structure and folding of intricately folded DNAs and RNAs. For instance, some categories of structural information, such as helix-stack preferences, are not easily accessed by using other low-tech, solution-based methods.

EXPERIMENTAL PROCEDURES

DNA Oligonucleotides

DNA oligomers were purchased from the University of Calgary Core DNA services. Oligomers were size purified on denaturing polyacrylamide gels. The procedure for coupling AQ to 5′-amino-C6-derivatized oligomers was as described in Fahlman and Sen [10]. DNA constructs were assembled by heating 5-fold concentrated solutions (2.5 μM of each DNA oligomer, trace of 5′-^{32}P-labeled E1, 100 mM Tris-HCl [pH 7.4]) at 100°C for 5 min, followed by slow cooling to 22°C. The solutions were transferred to the wells of a glycogen-pretreated, 96-well polystyrene plate just prior to photoirradiation.

Irradiation Experiments

The DNA solutions described above were diluted with aliquots from NaCl and/or $MgCl_2$ stock solutions to final salt concentrations of 50 mM NaCl and/or 1 mM $MgCl_2$. These solutions were incubated at 22°C for 15 min prior to the start of irradiation. All irradiations were carried out at 22°C, by using a UVP Black-Ray lamp (model UVL-56 with a 365 nm wavelength maximum, at 18 W), for 60 min; a distance of 1.7 cm separated the bulb and the DNA solution surface. After irradiation, the solutions were ethanol precipitated, and the resulting DNA pellets were dissolved in 10% (v/v) piperidine, prior to incubation at 90°C for 30 min. The treated DNA was lyophilized, dissolved in a standard denaturing loading buffer (pH 7.4) containing 5 mM EDTA, heat denatured at 90°C, cooled, and loaded on 15% (w/v) polyacrylamide sequencing gels. The band patterns from gels were analyzed by phosphorimagery, by using a Molecular Dynamics Typhoon 9410 Variable Mode Imager.

Mg^{2+} Titration

DNA solutions were heat denatured and cooled as described above; they were then made to final magnesium concentrations of 0–30 mM, equilibrated at room temperature (22°C) for 15 min, prior to initiation of irradiation.

Quenching Experiments with Ascorbic Acid

DNA solutions were prepared as for the magnesium titration experiments (above). L-ascorbic acid or ascorbic acid-6-palmitate (both from Sigma) was added to 50 μM, from stock solutions, to the appropriate DNA solutions prior to initiating irradiation. The L-ascorbic acid stock solution was prepared in ddH_2O. The ascorbic acid-6-palmitate stock solution was made up in DMSO. To equalize DMSO in all of the solutions to be irradiated, the 0 and 50 μM L-ascorbic acid-containing DNA solutions were made up to a final DMSO concentration of 0.185% (v/v) to match that present in the ascorbic acid-6-palmitate-containing DNA solutions.

Data Analysis

Densitometry of sequencing gels was carried out by using Molecular Dynamics Image Quant 5.2 software for Windows 2000. The density of a peak of interest, corresponding to damage at a particular nucleotide (e.g., G5), was assessed as a percentage of the total signal contained within that particular lane. This procedure compensated for slightly uneven loadings in different lanes. The normalized signal

for a particular nucleotide obtained in the "dark reaction" negative control lane was subtracted from the signal of the same nucleotide in an irradiated sample lane. Such a corrected signal for a particular nucleotide (e.g., G5) was then divided by the corrected signal for the reference nucleotide (G29) to give the damage ratio.

ACKNOWLEDGMENTS

We thank Carlo Sankar for his initial conceptualization of this work. We thank Peter Unrau for suggestions on the manuscript. This work was funded by the Canadian Institutes of Health Research (CIHR). D.S. is a Senior Scholar of the Michael Smith Foundation for Health Research.

Received: August 16, 2006
Revised: October 31, 2006
Accepted: November 6, 2006
Published: January 26, 2007

REFERENCES

1. Giese, B. (2002). Long-distance electron transfer through DNA. Annu. Rev. Biochem. *71*, 51–70.
2. Schuster, G.B. (2000). Long range charge transfer in DNA: transient structural distortions control the distance dependence. Acc. Chem. Res. *33*, 253–260.
3. Núñez, M.E., Hall, D.B., and Barton, J.K. (1999). Long-range oxidative damage to DNA: effects of distance and sequence. Chem. Biol. *6*, 85–97.
4. Henderson, P.T., Jones, D., Hampikian, G., Kan, Y., and Schuster, G.B. (1999). Long-distance charge transport in duplex DNA: the phonon-assisted polaron-like hopping mechansim. Proc. Natl. Acad. Sci. USA *96*, 8353–8358.
5. Joy, A., and Schuster, G.B. (2005). Long-range radical cation migration in DNA: investigation of the mechanism. Chem. Commun. 2778–2784.
6. Meggers, E., Michel-Beyerle, M.E., and Giese, B. (1998). Sequence dependent long range hole transport in DNA. J. Am. Chem. Soc. *120*, 12950–12955.
7. Ratner, M. (1999). Electronic motion in DNA. Nature *397*, 480–481.
8. Jortner, J., Bixon, M., Langenbacher, T., and Michel-Beyerle, M.E. (1998). Charge transfer and transport in DNA. Proc. Natl. Acad. Sci. USA *95*, 12759–12765.
9. Burrows, C.J., and Muller, J.G. (1998). Oxidative nucleobase modifications leading to strand scission. Chem. Rev. *98*, 1109–1151.
10. Fahlman, R.P., and Sen, D. (2002). DNA conformational switches as sensitive electronic sensors of analytes. J. Am. Chem. Soc. *124*, 4610–4616.
11. Odom, D.T., Dill, E.A., and Barton, J.K. (2001). Charge transport through DNA four-way junctions. Nucleic Acids Res. *29*, 2026–2033.
12. Fahlman, R.P., Sharma, R.D., and Sen, D. (2002). The charge conduction properties of DNA holliday junctions depend critically on the identity of the tethered photooxidant. J. Am. Chem. Soc. *124*, 12477–12485.
13. Santhosh, U., and Schuster, G.B. (2003). Long-distance radical cation reactions in DNA three-way junctions: inter-arm interaction and migration through the junction. Nucleic Acids Res. *31*, 5692–5699.
14. Bhattacharya, P.K., and Barton, J.K. (2001). Influence of intervening mismatches on long-range guanine oxidation in DNA duplexes. J. Am. Chem. Soc. *123*, 8649–8656.
15. Hall, D.B., and Barton, J.K. (2001). Sensitivity of DNA-mediated electron transfer to the intervening stack: a probe for the integrity of the DNA base stack. J. Am. Chem. Soc. *123*, 5045–5046.
16. Sankar, C.G., and Sen, D. (2004). DNA helix-stack switching as the basis for the design of versatile deoxyribosensors. J. Mol. Biol. *340*, 459–467.
17. Robertson, S.A., Harada, K., Frankel, A.D., and Wemmer, D.E. (2000). Structure determination and binding kinetics of a DNA aptamer-argininamide complex. Biochemistry *39*, 946–954.
18. Doudna, J.A., and Cech, T.R. (2002). The chemical repertoire of natural ribozymes. Nature *418*, 222–228.
19. Winkler, W.C., Nahvi, A., Roth, A., Collins, J.A., and Breaker, R.R. (2004). Control of gene expression by a natural metabolite-responsive ribozyme. Nature *428*, 281–286.
20. Faulhammer, D., and Famulok, M. (1996). The Ca^{2+} ion as a cofactor for a novel RNA-cleaving deoxyribozyme. Angew. Chem. Int. Ed. Engl. *35*, 2837–2841.
21. Santoro, S.W., and Joyce, G.F. (1997). A general purpose RNA-cleaving DNA enzyme. Proc. Natl. Acad. Sci. USA *94*, 4262–4266.
22. Feldman, A.R., and Sen, D. (2001). A new and efficient DNA enzyme for the sequence-specific cleavage of RNA. J. Mol. Biol. *313*, 283–294.
23. Peracchi, A. (2005). DNA catalysis: potential, limitations, open questions. ChemBioChem *6*, 1316–1322.
24. Silverman, S.K. (2005). In vitro selection, characterization, and application of deoxyribozymes that cleave RNA. Nucleic Acids Res. *33*, 6151–6163.
25. Egli, M. (2004). Nucleic acid crystallography: current progress. Curr. Opin. Chem. Biol. *8*, 580–591.
26. Liu, J., and Lu, Y. (2002). FRET study of a trifluorophore-labeled DNAzyme. J. Am. Chem. Soc. *124*, 15208–15216.
27. Cruz, R.P.G., Withers, J.B., and Li, Y. (2004). Dinucleotide junction cleavage versatility of 8–17 deoxyribozyme. Chem. Biol. *11*, 57–67.
28. Silverman, S.K. (2004). Breaking up is easy to do (if you're a DNA enzyme that cleaves RNA). Chem. Biol. *11*, 7–8.
29. Peracchi, A., Bonaccio, M., and Clerici, M. (2005). A mutational analysis of the 8–17 deoxyribozyme core. J. Mol. Biol. *352*, 783–794.
30. Peracchi, A. (2000). Preferential activation of the 8–17 deoxyribozyme by Ca(2+) ions. Evidence for the identity of 8–17 with the catalytic domain of the Mg5 deoxyribozyme. J. Biol. Chem. *275*, 11693–11697.
31. Brown, A.K., Li, J., Pavot, C.M.B., and Lu, Y. (2003). A lead-dependent DNAzyme with a two-step mechanism. Biochemistry *42*, 7152–7161.
32. Li, J., Zheng, W., Kwon, A.H., and Lu, Y. (2000). *In vitro* selection and characterization of a highly efficient Zn(II)-dependent RNA-cleaving deoxyribozyme. Nucleic Acids Res. *28*, 481–488.
33. Bonaccio, M., Credali, A., and Peracchi, A. (2004). Kinetic and thermodynamic characterization of the RNA-cleaving 8–17 deoxyribozyme. Nucleic Acids Res. *32*, 916–925.
34. Armitage, B., Yu, C., Devadoss, C., and Schuster, G.B. (1994). Cationic anthraquinone derivatives as catalytic DNA photonucleases–mechanisms for DNA damage and quinone recycling. J. Am. Chem. Soc. *116*, 9847–9859.
35. Dohno, C., Ogawa, A., Nakatani, K., and Saito, I. (2003). Hole trapping at N6-cyclopropyldeoxyadenosine suggests a direct contribution of adenine bases to hole transport through DNA. J. Am. Chem. Soc. *125*, 10154–10155.
36. Shao, F., O'Neill, M.A., and Barton, J.K. (2004). Long-range oxidative damage to cytosines in duplex DNA. Proc. Natl. Acad. Sci. USA *101*, 17914–17919.
37. Cadet, J., Berger, M., Douki, T., and Ravanat, J.-L. (1997). Oxidative damage to DNA: formation, measurement, and biological significance. Rev. Physiol. Biochem. Pharmacol. *131*, 1–87.

38. Cadet, J., Ravanat, J.-L., Buchko, G.W., Yeo, H.C., and Ames, B.N. (1994). Singlet oxygen DNA damage: chromatographic and mass spectrometric analysis of damage products. Methods Enzymol. *234*, 79–88.

39. Cadet, J., Douki, T., Pouget, J.-P., and Ravanat, J.-L. (2000). Singlet oxygen DNA damage products: formation and measurement. Methods Enzymol. *319*, 143–153.

40. Cadet, J., Ravanat, J.-L., Martinez, G.R., Medeiros, M.H.G., and Di Mascio, P. (2006). Singlet oxygen oxidation of isolated and cellular DNA: product formation and mechanistic insights. Photochem. Photobiol. *82*, 1219–1225.

41. Perrotta, A.T., Shih, I., and Been, M.D. (1999). Imidazole rescue of a cytosine mutation in a self-cleaving ribozyme. Science *286*, 123–126.

42. Nakano, S., Chadalavada, D.M., and Bevilacqua, P.C. (2000). General acid-base catalysis in the mechanism of an HDV ribozyme. Science *287*, 1493–1497.

43. Fiala, E.S., Conaway, C.C., Biles, W.T., and Johnson, B. (1987). Enhanced mutagenicity of 2-nitropropane nitronate with respect to 2-nitropropane—possible involvement of free radical species. Mutat. Res. *179*, 15–22.

44. Anwar, W.A., Au, W.W., Legator, M.S., and Ramanujam, V.M. (1989). Effect of dimethyl sulfoxide on the genotoxicity and metabolism of benzene in vivo. Carcinogenesis *10*, 441–445.

45. Odom, D.T., and Barton, J.K. (2001). Long-range oxidative damage in DNA/RNA duplexes. Biochemistry *40*, 8727–8737.

46. O'Neill, M.A., and Barton, J.K. (2002). 2-Aminopurine: a probe of structural dynamics and charge transfer in DNA and DNA:RNA hybrids. J. Am. Chem. Soc. *124*, 13053–13066.